

Tidal and Magnetic Interactions between a Hot Jupiter and its Host Star in the Magnetospheric Cavity of a Protoplanetary Disk

S.-H. Chang^{1,2} and P.-G. Gu¹

and

P. H. Bodenheimer³

ABSTRACT

We present a simplified model to study the orbital evolution of a young hot Jupiter inside the magnetospheric cavity of a proto-planetary disk. The model takes into account the disk locking of stellar spin as well as the tidal and magnetic interactions between the star and the planet. We focus on the orbital evolution starting from the orbit in the 2:1 resonance with the inner edge of the disk, followed by the inward and then outward orbital migration driven by the tidal and magnetic torques as well as the Roche-lobe overflow of the tidally inflated planet. The goal in this paper is to study how the orbital evolution inside the magnetospheric cavity depends on the cavity size, planet mass, and orbital eccentricity. In the present work, we only target the mass range from 0.7 to 2 Jupiter masses. In the case of the large cavity corresponding to the rotational period ≈ 7 days, the planet of mass > 1 Jupiter mass with moderate initial eccentricities ($\gtrsim 0.3$) can move to the region < 0.03 AU from its central star in 10^7 years, while the planet of mass < 1 Jupiter mass cannot. We estimate the critical eccentricity beyond which the planet of a given mass will overflow its Roche radius and finally lose all of its gas onto the star due to runaway mass loss. In the case of the small cavity corresponding to the rotational period ≈ 3 days, all of the simulated planets lose all of their gas even in circular orbits. Our results for the orbital evolution of young hot Jupiters may have the potential to explain the absence of low-mass giant planets inside ~ 0.03 AU from their dwarf stars revealed by transit surveys.

Subject headings: planetary systems: protoplanetary disks — stars: pre-main sequence

¹Institute of Astronomy and Astrophysics, Academia Sinica, Taipei 10617, Taiwan, R.O.C.

²Graduate Institute of Astrophysics, National Taiwan University, Taipei 10617, Taiwan, R.O.C.

³UCO/Lick Observatory, University of California, Santa Cruz, CA 95064, U.S.A.

1. Introduction

The number of discovered extrasolar planets has been increasing quickly¹ since the first extrasolar planet, 51 Pegasi b, was detected around a solar-type star (Mayor & Queloz 1995). 51 Pegasi b is the prototype of a class of exoplanets known as “hot Jupiters” because they are generally Jupiter-mass planets located $\lesssim 0.1$ AU from their parent stars and therefore their equilibrium temperatures are much higher than that of Jupiter. The high temperature of the protoplanetary disk at the orbital radii where they are now provides an environment extremely different from where giant planets are expected to form via either the core-accretion model (Pollack et al. 1996; Kokubo & Ida 2002) or the gravitational instability model (Gammie 2001; Boss 2004; Rafikov 2005). One of the most commonly adopted solutions is that hot Jupiters have formed at larger orbital radii in the protoplanetary disk and then moved inward to their current locations via the disk-planet interactions (e.g. Lin et al. 1996).

The magnetic fields of Classical T Tauri stars (hereafter CTTS) are typically strong enough to truncate the inner regions of protoplanetary disks to the corotation radius, where the Keplerian angular velocity of the disk is the same as the stellar-spin angular velocity, and create an inner magnetospheric cavity. Besides, the migration due to the planet-disk interaction is expected to slow dramatically once a young hot Jupiter passes the inner disk edge (Lin et al. 1996). The pile-up population of hot Jupiters at ~ 0.04 AU from their solar-type parent stars revealed from radial-velocity searches (Gaudi et al. 2005) may be attributed to the existence of the cavity (Carr 2007, and references therein).

On one hand, an attempt has been made by Setiawan et al. (2008) to search for a hot Jupiter around a CTTS, although Huélamo et al. (2008) substituted an explanation of a cool stellar spot for an orbiting hot Jupiter. Future observations will provide more evidence for planets of early ages. On the other hand, the simulated orbital evolution of giant planets as they migrate into the cavity was carried out by Rice et al. (2008). Their results suggest that high-mass hot Jupiters would move closer to their central stars and even be destroyed because planet’s entry into the magnetospheric cavity results in a growth in orbital eccentricity e . Although the eccentricity excitation is subject to the uncertain properties such as disk mass and viscosity, this model may provide a mechanism to pump up the eccentricity of a hot Jupiter inside the cavity and in turn affect the orbital evolution of the planet via the tidal interactions between the star and planet. In addition, the magnetic interactions between the star and planet in the magnetospheric cavity would be important as well, which may be an upscale analogy to the magnetic interactions between Jupiter and the Galilean satellites (Zarka 2007, and references therein).

The coupled tidal evolution of the radius and orbit of hot Jupiters in the absence of a disk has been investigated (Gu et al. 2003; Mardling 2007; Ibgui & Burrows 2009). To obtain noticeable influence on R_p , the tidal heating is assumed to be deposited deep in the planet in these models

¹ See the Extrasolar Planets Encyclopaedia (<http://exoplanet.eu>) for detail.

(Gu et al. 2004). The purpose of Mardling (2007) and Ibgui & Burrows (2009) is to explain the large radii of some transiting hot Jupiters using tidal heating. On the other hand, Gu et al. (2003) showed that for modest eccentricities, young hot Jupiters of radius ≈ 2 Jupiter radii at < 0.04 AU swell beyond two Jupiter radii and their internal degeneracy is partially lifted². Thereafter, their thermal equilibria become unstable and they undergo runaway inflation until their radii exceed the Roche radius. Then Roche lobe overflow ensues. Under the assumption that the overflowing gas immediately loses its orbital angular momentum to the planet and plunges into the central star, these mass-losing planets migrate outwards, such that their semi-major axes and Roche radii increase while their mass, eccentricity, and tidal dissipation rate decrease until the mass loss is quenched. Of course, including a disk would change the orbital evolutions of Roche-lobe-overflowing planets, as has been calculated by Trilling et al. (1998) who do not consider the tidal expansion of R_p and the magnetospheric cavity though.

As more and more hot Jupiters located $\lesssim 0.04$ AU have been discovered by transit surveys for recent years, it is noteworthy that almost no giant planets of mass < 1 Jupiter mass (M_j) have been detected within ~ 0.03 AU from their solar-type parent stars (see Figure 1; also see Udry & Santos 2007, and references therein). This puzzle may be attributed to the subsequent evolutions of hot Jupiters after they enter the magnetospheric cavity of the protoplanetary disk. Since thermal evaporation (e.g. Davis & Wheatley 2009) has not been undoubtedly identified to be the major cause (Murray-Clay et al. 2009, and references therein), we shall discuss the potential implication of our model to explain the observation in the end of the paper.

For the above reasons, in this work we concentrate on the orbital evolution of a young hot Jupiter inside the magnetospheric cavity of a protoplanetary disk by taking into account the tidal and magnetic interactions between the star and planet. To restrict to the problem without significantly involving the planet-disk interaction for simplicity, we consider the evolution after the hot Jupiter enters the 2:1 orbital resonance with the inner edge of a disk. The initial eccentricity, which is expected to be excited in the cavity before the planet migrates to the resonance location, is treated as one of the free parameters of the problem. The equations for the orbital and interior evolution of a hot Jupiter inside a magnetospheric cavity are described in §2. The results are presented in §3, and are summarized and discussed in §4.

2. Model Description

Figure 2 illustrates our toy model that shows a hot Jupiter orbiting a CTTS in a magnetospheric cavity of a protoplanetary disk. The magnetic dipole fields of a protostar truncate the inner part of the protoplanetary disk at the disk radius R_{mdisk} , which is the radius of the cavity. The initial

²For comparison, the initial orbits and eccentricities of a young hot Jupiter in Ibgui & Burrows (2009) are larger. Therefore the tidal heating in their model can proceed at a modest rate to attain the large R_p on the timescale of \sim Gyrs.

orbit of the planet is set to lie at the 2:1 orbital resonance with the inner edge of the disk, which allows us to ignore the tidal interactions between the disk and the planet (Lin et al. 1996; Rice et al. 2008). The semi-major axis a of this resonant orbit is denoted as $a_{2:1}$. However, when the inner edge of the disk extends inwards for any reasons in our model such that $a > a_{2:1}$, the planet is artificially moved inwards as well to maintain the 2:1 orbital resonance with the inner edge of the disk. Moreover, we assume that there is no magnetic linkage between the disk and the planet as illustrated in Figure 2 and therefore neglect magnetic interactions between them. In other words, the planet’s orbit evolves due to tidal and magnetic interactions with the central star, whereas the star interacts with both the planet and the disk. Therefore, this section consists of two parts, namely the magnetic and tidal effects, to describe the model in detail. §2.1 and §2.2 describe the star-disk and star-planet magnetic interactions, which leads to disk locking and contributes to the orbital evolution of the planet, respectively. §2.3 and §2.4 then describe the tidal interactions between the CTTS and the planet. The circularization of the planet’s orbit is due to tides on both the planet and the star. The thermal inflation of the planet is due to tides on the planet excited by the star. On the other hand, the tides on the star raised by the planet affect the evolution of the planet’s orbit and the stellar spin. Finally, we summarize the key formulae for our model in §2.5.

2.1. Star-Disk Magnetic Interaction

There have been a number of models for the star-disk interactions to account for the rotation of CTTSs as well as star and jet formation (e.g. Shu et al. 1994; Matt & Pudritz 2005; Lovelace et al. 2008). In addition to the closed field lines connecting from the protostar to the disk to allow for funnel accretion, the open field lines may diverge primarily from the inner edge of the disk (i.e. X-wind model, see Shu et al. 1994) or emanate largely from the star and the disk (i.e. stellar and disk wind model, see Matt & Pudritz 2005). Furthermore, the stellar field topology may be in the complex form of multipole (Lovelace et al. 2008) or tilted dipole relative to the stellar spin (Laine et al. 2008). In this work, we ignore these complications and adopt the simple non-tilted dipole configuration of stellar fields that thread through the protoplanetary disk as has been illustrated in Figure 2.

To calculate the magnetic torque T_{mag} on the star due to the magnetic linkage to the disk, we adopt the approach by Armitage & Clarke (1996) in which the magnetic torque acting on an annulus of the disk is due to the azimuthal twisted field lines B_ϕ caused by the difference between the stellar spin and the orbital motion of the annulus (Livio & Pringle 1992). Hence, the torques integrated from the disk inner edge at R_{mdisk} to infinity contribute to the net magnetic torque between the star and the disk:

$$T_{mag} = \frac{\mu^2}{3}(R_{mdisk}^{-3} - 2R_c^{-3/2}R_{mdisk}^{-3/2}), \quad (1)$$

where $\mu = B_*R_*^3$ is the stellar dipole moment, B_* is the magnetic field strength at the stellar surface, R_* is the stellar radius, $R_c = (GM_*/\Omega_*^2)^{1/3}$ is the corotation radius, Ω_* is the stellar spin

rate, and M_* is the stellar mass. We employ the same scaling law as used in Armitage & Clarke (1996) to specify the strength of stellar magnetic field:

$$B_* = B_0 \left(\frac{4\text{days}}{2\pi/\Omega_*} \right), \quad (2)$$

where the scaling factor B_0 is a constant indicative of the surface magnetic strength for the stellar spin period of 4 days.

The magnetospheric radius R_{mdisk} is determined by the balance between the stellar magnetic stress and the disk Reynolds stress (Starczewski et al. 2007, and references therein):

$$R_{mdisk} = \eta \left(\frac{B_*^4 R_*^{12}}{GM_* \dot{M}_{disk}^2} \right)^{1/7}, \quad (3)$$

where \dot{M}_{disk} is the disk accretion rate and η is a dimensionless factor of order unity. For a star with an aligned dipole field, $0.5 \leq \eta \leq 1.0$. In addition, the mass transfer rate throughout the disk is assumed to be comparable to an observational inferred accretion rate from protostellar disks onto CTTSs, which decays with time t over the timescale $\sim 10^7$ years and can be fitted by

$$\dot{M}_{disk} = 10^{-4} \frac{M_\oplus}{\text{yr}} \left(\frac{t}{10^7 \text{yr}} \right)^{-3/2}, \quad (4)$$

where M_\oplus is the Earth mass (Ida & Lin 2004).

The equation for the spin evolution of the protostar is then given by

$$\frac{d\Omega_*}{dt} = -\frac{1}{I_*} (\dot{I}_* \Omega_* - T_{disk}). \quad (5)$$

In the above equation, \dot{I}_* is the moment inertia of the CCTS and $T_{disk} = T_{mag} + T_{acc}$ is the net torque arising from the presence of the disk, where T_{acc} is the torque spinning up the star due to the disk accretion:

$$T_{acc} = \dot{M}_{disk} R_{mdisk}^2 \Omega_{disk}, \quad (6)$$

with Ω_{disk} being the Keplerian angular speed at the radius R_{mdisk} (Armitage & Clarke 1996; Matt & Pudritz 2005). R_* and \dot{I}_* are obtained from the interior structure of the contracting CTTS modeled by Armitage & Clarke (1996), who modified the Eggleton code (Pols et al. 1995) for the pre-main sequence evolution.

When the star rotates faster than the inner edge of the disk (i.e. $\Omega_* > \Omega_{disk}$), the mass accreting onto the star should be ceased by the centrifugal force and T_{acc} is therefore set to be zero in our model. Meanwhile, the star experiences immediate magnetic braking as a result of its strong fields, leading to disk locking of the stellar spin. Disk locking makes the star and the inner disk edge

corotate again and resumes the accretion. Therefore precisely speaking, the disk density near the inner edge of the disk, R_{mdisk} , and \dot{M}_{disk} should fluctuate with time. In practice, we have simply employed equations (3) and (4) to implement the disk properties rather than modelling the detailed disk structure near R_{mdisk} . This is certainly a limitation of our model. With regard to the overall disk accretion rate, as we shall see in §3, the fluctuation of the balance between the mass accretion and the magnetic braking (i.e. disk locking) is rather fast compared to the timescales of interest, meaning that equation (4) is a proper approximation to describe the average mass accretion rate in our problem.

2.2. Star-Planet Magnetic Interaction

The torque on the planet due to magnetic linkage to the star is modelled as the magnetic stress ($B_z B_\phi / 4\pi$) multiplied by the cross-sectional area of the planet's magnetosphere and the distance r between the planet and its parent star. It is assumed that the planet has a magnetosphere in which the gas behaves like plasma. In addition, the magnetosphere is assumed to be as large as the planet's size, so the area of the planet interacting with the stellar field is $2\pi R_p^2$. Applying the star-disk magnetic interaction described in §2.1 to the star-planet case, we obtain the magnetic torque on the planet

$$T_{planet} = \frac{B_*^2 R_*^6 R_p^2}{2} \left(\frac{1}{r^5} - \frac{\Omega_*}{r^5 \dot{\phi}} \right), \quad (7)$$

where $\dot{\phi}$ is the orbital angular velocity. The magnetic torque changes with the distance between the planet and the central star while the planet moves in an eccentric orbit, so we employ the mean torque over one orbit period P_{orbit} . That is,

$$\int_0^{P_{orbit}} T_{planet} dt = \frac{B_*^2 R_*^6 R_p^2}{2} \int_0^{P_{orbit}} \left(\frac{1}{r^5} - \frac{\Omega_*}{r^5 \dot{\phi}} \right) dt. \quad (8)$$

To carry out the above integral, we make the approximation that the orbit does not vary significantly during one orbital period; i.e., the orbital angular velocity $\dot{\phi} \approx a^2 n \sqrt{1 - e^2} / r^2$ and $r \approx a(1 - e^2) / (1 + e \cos \phi)$, where a is the semi-major axis, e is the eccentricity, and n is the mean motion of the mutual orbit of the planet and the star. Then after integrating and being divided by P_{orbit} , equation (8) gives an expression for the mean magnetic torque on the planet:

$$\langle T_{planet} \rangle = \epsilon \frac{B_*^2 R_*^6 R_p^2}{4} \left[\frac{2 + 3e^2}{a^5 (1 - e^2)^{7/2}} - \frac{2\Omega_*}{a^5 n (1 - e^2)^2} \right]. \quad (9)$$

Here, we have introduced a coefficient ϵ , where $0 \leq \epsilon \leq 1$, to regulate the magnetic torque on the planet, a formulism similar to that applied to the magnetic torques between the Galilean satellites and Jupiter (Zarka 2007). In this regard, the energy dissipation associated with the magnetic torque can be generally considered as the Poynting flux at the magnetopause scaled by ϵ . Hence, $\epsilon = 1$ corresponds to the upper limit of the magnetic torque.

2.3. Tides on the Planet

The planet is assumed to have zero obliquity and zero orbital inclination. The gravitational tides on the planet affect the evolution of the eccentricity and the spin of the planet. For the sake of simplicity, we do not consider the influence of the planet-star magnetic interactions on the spin and eccentricity of the planet. Therefore, the rate of the eccentricity change of the orbit is due solely to gravitational tides on the planet and the star. The rate contributed from the tidal dissipation in the planet alone is given by g_p , which can be obtained from (Mardling & Lin 2002)

$$g_{p,*} = -\frac{81e}{2Q'_{p,*}} \left(\frac{M_{*,p}}{M_{p,*}} \right) \left(\frac{R_{p,*}}{a} \right)^5 \left[f_1(e)n - \frac{11f_2(e)\Omega_{p,*}}{18} \right], \quad (10)$$

where g_* for the tidal dissipation in the star is also shown and will be considered in §2.4. In the above equation, $f_1(e) = (1+15e^2/4+15e^4/8+5e^6/64)/(1-e^2)^{13/2}$ and $f_2(e) = (1+3e^2/2+e^4/8)/(1-e^2)^5$. Moreover, Q'_* and Q'_p are the tidal quality factors of the star and the planet, respectively. All the uncertainties associated with the physical processes of tidal heating are contained in the Q' values. For a fiducial value, it has been suggested that the Q'_p values inferred for Jupiter from Io's orbital evolution is $5 \times 10^4 < Q'_p < 2 \times 10^6$ (Yoder & Peale 1981). With this Q'_p value, orbits of planets with M_p and R_p comparable to those of Jupiter and with a period less than a week, are circularized within the main-sequence life span of solar-type stars. Q'_* has been inferred to be $\sim 1.5 \times 10^5$ for the very young binary stars (Lin et al. 1996).

Since the synchronous timescale of the planet is much shorter than the circularization timescale (Gu et al. 2003), we simply assume that the planet's spin equals the orbital rotation throughout the evolution. This assumption may be invalid during the phase of the Roche-lobe overflow if the orbit changes dramatically due to quick mass loss (see eq. (15) below), causing a large discrepancy between the planet spin and orbital motion. This means that the tidal heating due to synchronization is unrealistically ignored during this special phase in our model.

Moreover, the tidal process of orbital circularization shrinks the planet's orbit; i.e.,

$$\dot{a} = \frac{2e\dot{e}}{1-e^2}a. \quad (11)$$

During the orbital circularization, there is substantial tidal heating within the planet. The tidal heating of the planet may have contributed significantly to the thermal budget that governs the planet's physical properties, including its radius (Bodenheimer et al. 2001; Gu et al. 2003, 2004; Mardling 2007; Ibgui & Burrows 2009).

Ignoring the rotation energy of the planet, we can write the first law of the thermodynamics for a tidally heated planet as follows:

$$\dot{E}_{tide} - \mathcal{L} = \dot{U} + \dot{W}, \quad (12)$$

where \dot{E}_{tide} is the tidal heating rate (see Mardling & Lin 2002 for the expression), \mathcal{L} is the intrinsic luminosity from the photosphere of the planet, U is the internal energy, and W is the gravitational

potential energy. Suppose that $U = q_U GM_p^2/R_p$ and $W = -q_W GM_p^2/R_p$ with the coefficients q_U and q_W depending on the interior structure of the planet. Then in the absence of mass loss (i.e. $\dot{M}_p = 0$), the above energy equation gives rise to the expansion/contraction rate of the planet (cf. Mardling & Lin 2002)³:

$$\left(\frac{\partial R_p}{\partial t}\right)_{\dot{M}_p=0} = \frac{\dot{E}_{\text{tide}} - \mathcal{L}}{\left(\frac{d \ln q_U}{d \ln R_p} - 1\right) \frac{U}{R_p} - \left(\frac{d \ln q_W}{d \ln R_p} - 1\right) \frac{W}{R_p}}. \quad (13)$$

Even though the expanding/contracting planet is not in the thermal equilibrium, q_U , q_W , and \mathcal{L} can be simply expressed in terms of functions of R_p and M_p as long as the timescales under consideration are $>$ the convective turnover time for an almost convective planet with the same solid-core mass and a thin radiative envelope of the same opacity (i.e. an almost polytropic interior, see Gu et al. 2003, 2004). In our approach, the core mass of the planet is assumed to be $19.4M_\oplus$, which is motivated by the core accretion model for the formation of giant planets (Pollack et al. 1996). However, the thermal properties of the core are not modelled in our work. $q_U(R_p)$, $q_W(R_p)$, and $\mathcal{L}(R_p)$ are obtained only from certain different M_p by fitting to the numerical data for the interior structures of tidally inflated Jupiters described in Gu et al. (2003). Subsequently, their values and derivatives with respect to R_p for any desired M_p can be interpolated from these available fitted functions.

Once the planet’s radius exceeds its Roche radius R_l (see the Appendix), the mass loss ensues. During the planet overflow phase, the R_p adjustment after losing mass plays an important role in determining the subsequent evolution. R_p changes with M_p as well according to the equation of state of the planet even though the entropy of the planet does not change. Since the interpolated data derived from our interior structure code is unable to deal with the processes that are as quick as the adiabatic mass loss, we adopt the following simple methodology. Assuming a polytropic structure of a planet, the adiabatic mass-radius exponent $\alpha \equiv (\partial \ln R_p / \partial \ln M_p)_s$ can be estimated from the polytropic index of the planet (Gu et al. 2004). α can then be related to the gravitational potential energy. It can be easily shown that $\alpha = (3 - 4q_W)/(3 - 2q_W)$. For simplicity we shall use this relation to estimate α from q_W for a Roche-lobe filled planet, albeit these polytropic relations are derived for an isolated gravitationally bound body. Therefore, the complete expression of \dot{R}_p in the presence of the mass loss through the Lagrangian 1 (L1) point should read

$$\dot{R}_p = \left(\frac{\partial R_p}{\partial t}\right)_{\dot{M}_p=0} + \alpha \left(\frac{R_p}{M_p}\right) \dot{M}_p, \quad (14)$$

where we shall adopt the formalism in Kolb & Ritter (1990) to estimate \dot{M}_p (see §2.5 for the detail). In the case of a giant planet with large radius such as a young hot Jupiter, α is always negative. In addition, $|\alpha|$ increases with R_p , because the planet degeneracy is being lifted when its density goes down (Gu et al. 2004).

³The internal energy is ignored in Mardling & Lin (2002)

Similar to the physical condition for the formation of the magnetospheric cavity of the disk, planet’s overflow may either form a ring/disk or funnel along the stellar field lines onto the CTTS depending on whether \dot{M}_p is strong enough to dominate over the stellar fields. Therefore, we modify equation (3) by replacing \dot{M}_{disk} with \dot{M}_p to define the “overflow cavity radius R_{oc} ” where the Reynolds stress of the overflowing gas is comparable to the magnetic stress of the stellar fields. Thus, if this radius is larger than planet’s semi-major axis, where the overflow occurs, the overflowing gas will flow through the magnetic field to the central star. The stellar spin will speed up under the action of the torque from planet’s overflow, $T_{\dot{M}_p} = \dot{M}_p(GM_*a)^{1/2}$, which is an analogy to the spin-up torque due to the disk accretion described in equation (6). This leads to the evolution of the stellar spin caused by the planet’s overflow:

$$\frac{d\Omega_*}{dt} = \frac{1}{I_*} \dot{M}_p (GM_*a)^{1/2}. \quad (15)$$

On the other hand, if the overflow cavity radius is smaller than the semi-major axis, the overflowing gas will form a ring/disk around the star instead of directly funnelling along the field lines onto the star. In this stage, we assume that the total angular momentum of the overflowing gas is immediately transferred to the orbit of the planet, leading to the outward migration of the mass-losing planet:

$$\left(\frac{da}{dt}\right)_{overflow} = -\frac{2\dot{M}_p a}{M_p}, \quad (16)$$

and therefore no spin-up torque is exerted on the star.

The above equation for outward migration suggests that the mass-losing planet can be detached from its Roche lobe as long as R_p does not expand as fast as R_l . Therefore, it is worthwhile to examine the linear stability of a Roche-lobe filled planet against mass loss. The definition of R_l from the Appendix and equation (16) give $\dot{R}_l/R_l = (-5/3)(\dot{M}_p/M_p)$. Equation (14) then indicates that the expansion rate of R_p is $\approx -\alpha\dot{M}_p/M_p$ provided that the thermal adjustment of R_p is less important than the adjustment of R_p due to the adiabatic mass loss. Once the planet’s photosphere reaches the Roche radius (i.e. $R_p = R_l$), the above analysis infers that the mass loss of a Roche-lobe filled planet is linearly unstable (i.e. undergoes exponential growth) if $|\alpha| > 5/3$.

2.4. Tides on the Star

In addition to the tides on the planet induced by the star, the planet also raises the tides on the star to circularize the orbit and to lock the rotation of the star.

The circularization rate described in the preceding subsection has to be complemented by the tidal dissipation in the star; namely,

$$\frac{de}{dt} = g_p + g_*, \quad (17)$$

where g_* has been displayed in equation (10).

The process of the tidal locking of the CTTS leads to the exchange of the angular momentum between the planet’s orbit and stellar spin. The stellar spin is assumed to be normal to the orbital plane of the planet and the disk. Owing to this tidal effect, the angular momentum of the stellar spin changes at the rate (Mardling & Lin 2002)

$$\dot{J}_* = \left(\frac{9J_0M_p}{M_t} \right) \left(\frac{f_4(e)\Omega_* - f_3(e)n}{2Q_*'(1-e^2)^{1/2}} \right) \left(\frac{R_*}{a} \right)^5, \quad (18)$$

where $J_0 = M_p[GM_t a(1-e^2)]^{1/2}$ is the total angular momentum of the planet’s orbit, $f_3(e) = (1 + 15e^2/2 + 45e^4/8 + 5e^6/16)(1-e^2)^{-6}$, and $f_4(e) = (1 + 3e^2 + 3e^4/8)(1-e^2)^{-9/2}$. The evolution of stellar spin associated with equation (18) is then given by

$$\dot{\omega}_* = \left(\frac{M_p^2}{I_*M_t} \right) \left(\frac{9n}{2Q_*'} \right) \left(\frac{R_*^5}{a^3} \right) [f_3(e)n - f_4(e)\Omega_*]. \quad (19)$$

2.5. Equations for simulation

After describing the various interactions separately, we list and recapitulate the final equations incorporating these interactions for solving the orbital evolution of a young hot Jupiter in a magnetospheric cavity.

The rate of orbital circularization (i.e. eq. (17)) is given by

$$\frac{de}{dt} = g_p + g_*.$$

The evolution of planet’s size (i.e. eq. (14)) has the form

$$\dot{R}_p = \left(\frac{\partial R_p}{\partial t} \right)_{\dot{M}_p=0} + \alpha \left(\frac{R_p}{M_p} \right) \dot{M}_p.$$

The first term on the right side is due to thermal adjustment, whereas the second term is due to Roche-lobe overflow driven by an adiabatic process that occurs much faster than the first term.

When $R_p > R_l$, the mass loss occurs in our simulation. This implicitly implies that we neglect the mass loss from the optically thin atmosphere before the planet’s photosphere reaches its Roche radius. We also ignore the possible mass loss through the L2 point (Gu et al. 2003). The mass-loss rate of the planet is estimated from the 1-D interior structure of the planet along with the formula in Kolb & Ritter 1990 (and see the definitions of the notations therein):

$$\dot{M}_p = 2\pi F_1(q) \frac{a^3}{GM_*} \int_{\Phi_L}^{\Phi_{ph}} F_3(\Gamma_1) \left(\frac{RT}{\mu} \right)^{1/2} \rho d\Phi. \quad (20)$$

The orbital decaying rate of the planet is given by

$$\frac{da}{dt} = \frac{2ae\dot{e}}{1-e^2} - \frac{2 \langle T_{planet} \rangle}{M_p a n \sqrt{1-e^2}} + \frac{2a\dot{J}_*}{J_0} - \frac{2\dot{M}_p a}{M_p}. \quad (21)$$

The first term on the right side represents the orbital decay due to circularization (i.e. eq. (11)). The second term is due to the magnetic torque on the planet (i.e. eq. (9)) and the third term arises from tides on the star (i.e. eq. (18)). The last term is included only when the overflow occurs (i.e. eq. (16)). Moreover, when R_{disk} shrinks such that the 2:1 resonance location lies in the disk, the planet is expected to slowly migrate inwards (Rice et al. 2008). However, when this happens, we assume just for the sake of simplicity that a is decreased instantaneously to maintain the 2:1 resonance with the inner edge of the disk.

The stellar spin evolution is determined by a number of factors:

$$\frac{d\Omega_*}{dt} = -\frac{1}{I_*} \{ \dot{I}_* \Omega_* - T_{disk} - \langle T_{planet} \rangle + \dot{M}_p [GM_* a (1 - e^2)]^{1/2} \} + \dot{\omega}_*. \quad (22)$$

The first term in the curly bracket arises from the evolution of the stellar moment of inertia during the pre-main-sequence phase and the second term represents the torque exerted by the disk on the star due to disk accretion and the magnetic linkage (i.e. eq. (5)). The third and the fourth terms are due to the magnetic linkages with the planet (i.e. eq. (9)) and the overflowing gas from the overfilled Roche lobe (i.e. eq. (15)), respectively. The last term $\dot{\omega}_*$ results from the tides on the star (i.e. eq. (19)).

3. Numerical Results

To solve the ODEs in the preceding section (eq. (17), (14), (20), (21), (22)), we employ the 4th order Runge-Kutta method to study the inward migration of a young hot Jupiter in the magnetospheric cavity due to tidal and magnetic interactions with its CTTS. The simulations start from $t = 10^5$ yr to 10^7 yr. The planet is not introduced to the orbit with $a = a_{2:1}$ until $t = 7 \times 10^5$ years, a timescale comparable to the Type II migration time of a giant planet in a proto-planetary disk (Lin & Papaloizou 1985).

In our model, B_0 , e , and M_p are parameterized to investigate the various evolutions of the planetary migration in the magnetospheric cavity. Besides, Q_*' , Q_p' and η are fixed as 3×10^5 , 10^6 , and 0.75 throughout the simulation.

The initial period of the central star is set to be 15 days at $t = 10^5$ years (see the left panel of Figure 3). The figure shows the stellar spin will be locked by the disk in a few $\times 10^4$ years and therefore the initial spin is insensitive to the tidal and magnetic interactions, which proceed on the timescales of $\sim 10^{5-6}$ years. The final disk-lock period (i.e. the Keplerian period of the disk inner edge) depends on the magnitude of the magnetic field of the central star (Armitage & Clarke 1996). We discuss two cases of cavity sizes corresponding to $B_0 = 1500\text{G}$ (§3.1) and $B_0 = 500\text{G}$ (§3.2) separately. The disk with a big cavity will lock the central star at the rotational period of ~ 7 days and that with a small cavity will lock it at ~ 3 days. Herbst & Mundt (2005) revealed the peculiar bimodal distribution of periods for young stars in the Orion Nebula Cluster. The distribution of periods at an age of about 1 Myr exhibit two peaks, one located at a period of about

8 days and the other at a period of about 2-3 days (Bouvier 2007). The disk-lock periods in our model approximately match the observation.

We consider the planets of four different planetary masses $2M_j$, $1.5M_j$, $1M_j$, and $0.7M_j$ to study their different evolutions of migration. From the observations, the close-in transiting giant planets have radii ranging from $\sim 0.8 R_j$ to $\sim 1.7R_j$. Thus $1.7R_j$ could be considered as a lower limit of the radius of a young Jupiter although some of the large planet’s sizes have been postulated to be attributed to tidal heating (Miller et al. 2009) or evaporation (Baraffe et al. 2004). Also, $1.7 R_j$ corresponds to the theoretical radius of a young Jupiter (Marley et al. 2007). Thus we fix the initial $R_p = 1.7R_j$ for all the cases.

When $t = 7 \times 10^5$ yr and the planet is introduced to the initial location at $a = a_{2:1}$, the star has been locked by the disk. The right panel of Figure 3 shows the decrease in the periods of stellar spin and planet’s orbit before $t \lesssim 10^6$ years. This is caused primarily by the contraction of the cavity as R_* decreases (see eq. (3)). Orbiting interior to the co-rotation radius, the planet then migrates inwards from the 2:1 resonance due to faster revolution of the planet than the spin of the central star. This is illustrated by the black curve during the time $t > 10^6$ years in the right panel of Figure 3 where the planet with $1M_j$ and $e_i = 0.16$ is used as an example. Meanwhile, the star should spin up via the tidal and magnetic interactions with the planet. However, the disk locking dominates the evolution of the stellar spin as indicated by the overlap between the red solid and blue dashed curves in the right panel of Figure 3. In other words, the inner edge of the disk acts as the sink of total angular momentum of the system in our model. In fact, the rotational period of the disk inner edge fluctuates slightly from the spin period of the star on short timescales. Nevertheless, these two periods are almost the same over long timescales, justifying the argument given in §2 that equation (4) is a proper approximation to describe the average mass accretion rate and determine the cavity size in our problem.

As mentioned in §2.3, the planet will lose its mass if the planet’s radius exceeds the Roche radius. However, if the planet’s mass decreases to 20 earth masses, the simulation will be forced to stop. This is because the core mass of a giant planet is 19.4 earth masses in our model.

3.1. The Large-Cavity Case

A large cavity is opened up by the strong stellar magnetic fields with the scaling factor $B_0 = 1500$ G. In this case, the planet starts to migrate from $a_i \sim 0.045$ AU, which corresponds to $a_{2:1}$ at $t = 7 \times 10^5$ years.

The migration evolutions of the planets with same masses will differ as a result of different initial eccentricities. The distance, over which the planet can migrate inward from the initial position, is shortest when $e_i = 0$ and increases as e_i increases. This is because firstly, the circularization of a eccentric orbit makes the orbit shrink. Secondly, the inflation of a planet due to tidal heating enhances the star-planet magnetic interaction. Also, the tidal torque on the star caused by the

planet is more significant as e_i is larger. All of the above factors accelerate the migration rate of the planet. When $e_i \geq$ the critical eccentricity e_c , the planet’s radius will exceed its Roche lobe and start to lose mass onto the central star.

We perform the calculations for three cases of e_i : (1) $e_i = 0$; (2) $e_i = e_c$; (3) $e_i = e_c - 0.01$ for each planet mass. The orbital evolutions are shown in Figure 4 and the explanations are presented below.

In the case of $e_i = 0$ (solid lines in the figure), the results for different masses are not significantly difference. Without an eccentric orbit to bring the planet closer to the central star (i.e. the perihelion), the tidal and magnetic effects are excited less effectively in a large distance between the planet and the central star. Hence, planets with different masses initially in circular orbits migrate to almost the same final positions, $a \sim 0.037$ AU at $t = 10^7$ yr, as the cavities contract and drive the planets to the 2:1 resonances.

When $e_i = e_c$ (dotted lines in the figure), the planets start to overflow their L1 points and lose mass. As shown in the figure, their evolutions are terminated before the end of the simulations ($t = 10^7$ years), suggesting that all of the planets are disrupted. The termination of the simulations occurs when the discrepancy between R_p and R_l is so large during the overflow phase that \dot{M}_p is too large to be resolved in the simulation with the time step = 100 years. This time step of 100 years is already shorter than the time step used for the interpolated data derived from our interior structure code. When the runaway solutions happen, $|\alpha|$ is always larger than 5/3, which is in agreement with the linear instability of the mass loss. For the 0.7 and $1M_j$ cases, the mass loss rate is high. The overflow gas is able to form a ring/disk and hence the planet migrates outward according to equation (16) in our model. However, once their overflows occur, $|\alpha| > 5/3$ at the same time owing to their large R_p . The radius adjustment is predominated by the adiabatic mass loss instead of tidal inflation, leading to the runaway solutions to the ODEs.

On the other hand for the $1.5M_j$ and $2M_j$ cases, they migrate fast to the locations closer to the central stars owing to the stronger tides raised by these massive planets on their central stars. In addition, these more massive planets are more difficult to inflate by tidal heating due to their higher gravitational binding energies and cooling rates (Gu et al. 2003, 2004). Hence, when they overflow their Roche lobes, R_p is not too large and therefore $|\alpha| < 5/3$, leading to the stable overflow. Although the overflowing gas initially funnels to the central star, the overflow rate becomes substantially high shortly such that $R_{oc} < a$. Consequently the massive planets have undergone outward migration almost since the overflow began. The outward migration is primarily driven by inward migration due to the tidal and magnetic interactions rather than tidal inflation. The overflow finally turns to be unstable when $|\alpha|$ increases to 5/3 as a and therefore R_p increases. The evolution then stops and the planet loses all its gas to the central star. During the phase of the fast outward migration, the planet’s spin may become unlocked with its orbital motion. Despite not being included in our model, the tidal heating associated with the asynchronism would speed up the planet inflation and lead to the same catastrophic fate of the planet. Comparing these cases

for different initial M_p , massive planets require higher e_c thus more tidal heating to be inflated against their greater gravitational binding energies and cooling rates. $M_p = 2M_j$ requires $e_c = 0.35$ and destructs at $a \sim 0.02$ AU, while $M_p = 0.7M_j$ needs $e_c = 0.22$ and destructs at $a \sim 0.035$ AU.

Now we turn to the case for $e_i = e_c - 0.01$ (i.e. e_i is slightly smaller than e_c) to study the conditions in which the planet of a given mass can migrate inward the farthest and still survive in the end of the simulation. As can be expected from the previous results for $e_i = e_c$, the dashed curves in the figure show that a more massive planet undergoes faster migration due to the stronger tidal torque. Thus, the planet with $M_p = 2M_j$ and $e_i = 0.34$ can arrive at $a \sim 0.024$ AU, while the planet of $M_p = 0.7$ and $1 M_j$ can not migrate to the region < 0.03 AU. Furthermore, a low mass planet is more easily inflated by tidal heating, giving rise to the relatively stronger magnetic interaction (see eq. (9)). This explains why the planet of $0.7M_j$ migrates slightly farther in than the planet of $1M_j$ in the end of the simulation.

In equation (9), the coefficient ϵ regulates the magnetic torque on the planet, and the upper limit $\epsilon = 1$ has been applied to obtain the above results. Here, we employ $\epsilon = 0$ to study the orbital evolutions in the absence of the magnetic torque. In comparison to the previous orbital evolutions shown in Figure 4, Figure 5 shows the lower migration rates because of the lack of the star-planet magnetic interaction for the $M_p = 0.7, 1, \text{ and } 1.5M_j$ cases. However, the stellar tides induced by the $2M_j$ planet are far dominant over the magnetic interaction, so the massive planet still migrates to $a \sim 0.016$ AU. That position is even farther inward than $a \sim 0.024$ AU for the $\epsilon = 1$ case as the planet with even higher $e_i = 0.38$ can still survive in the absence of the magnetic torque. Moreover, Figure 5 confirms the previous subtle result about the dependence of the magnetic torque on R_p : the slightly more inward migration of the planet of $0.7M_j$ than $1M_j$ does not reappear because there exists no magnetic torque to speed up inward migration for a lighter planet of a larger inflated radius. As to the cases for $e_i = e_c$, the simulated planets overflow their Roche radii and perish in the same way as in the $\epsilon = 1$ cases; namely, $|\alpha|$ of various cases finally is $> 5/3$ and the mass loss becomes runaway. For the cases of $0.7M_j, 1M_j, \text{ and } 1.5M_j$, $|\alpha| > 5/3$ once their overflow occurs. On the other hand, after reaching the Roche lobe, the planet of $2M_j$ migrates outward for a period of time due to stable overflow and inward migration driven by the tidal torque. It is finally destroyed due to the large $|\alpha|$ that increases with R_p as the mass-losing planet moves outwards.

3.2. The Small-Cavity Case

The weaker stellar fields due to the smaller scaling factor $B_0 = 500$ G form a smaller magnetospheric cavity, so the initial position of the planet is much closer to the central star; namely, $a_i \sim 0.032$ AU. The planet and the star exert remarkable tidal forces on each other in such short distances, and the magnetic torque on the planet is not negligible as well. R_l is getting smaller while the planet migrates inwards. As soon as $R_l < R_p$, the overflow occurs, leading to the destruction. Consequently, even $e_i = 0$ (i.e., no tidal heating in the planet), all the planets destruct irrespective of their mass. If M_p is bigger, the migration is faster due to the stronger tidal torque. Therefore,

the more massive the planet is, the quicker the planet destructs, as shown in Figure 6 for $\epsilon = 1$.

The orbital evolutions of the the $1M_j$ and $2M_j$ cases are characterized by the alternating out/inward orbital migrations. Once the overflow occurs, the large expansion of R_l due to the high mass loss rate dominates over the adiabatic inflation, hence leading to the fast outward migration. As a result, R_p temporarily detaches from R_l for a while until the planet moves in and the next Roche overflow occurs again. Finally, the planet will lose all its mass when the overflow occurs accompanied with high $|\alpha|$ (i.e. $> 5/3$).

In the absence of the magnetic torque (i.e. $\epsilon = 0$), the tides raised by massive planets on the stars still drive significant inward migration of the planets. Figure 6 shows that shutting down the magnetic torque cannot change the outcome of planet destruction for $M_p \geq 1M_j$. However, the planet of $0.7M_j$ can survive in 10^7 years because the inward migration driven by the weak tidal torque from the low mass planet is slow. Therefore, we estimate $e_c = 0.18$ for the planet to perish and show the evolution in the leftmost panel of Figure 6.

4. Summary and Discussion

We construct a simple model to study the orbital evolution of a young hot Jupiter in an eccentric orbit inside a magnetospheric cavity of a proto-planetary disk around a CTTS. For the sake of simplicity, we assume that the magnetospheric cavity of the protoplanetary disk is truncated by a stellar dipole field. Through the magnetic linkage between the central star and the disk, the rotational period of the star is quickly locked by the inner edge of disk. We then introduce a young hot Jupiter at $a_{2:1}$ and restrict ourselves to the orbital evolution of a hot Jupiter inside the cavity. Assuming that the planet behaves like a plasma, we apply the same formulism for the star-disk magnetic interaction to that for the star-planet interactions. We adopt the equilibrium-tide equations with $Q_* = 3 \times 10^5$ and $Q_p = 10^6$ to model the star-planet tidal interactions. In so doing, our model focuses on the planet migration due to tidal and magnetic interactions between the planet and the star, and does not consider any interactions between the planet and the disk. However, as the size of the magnetospheric cavity evolves, the planet is artificially pushed to $a_{2:1}$ if it lies beyond $a_{2:1}$. We vary three parameters B_0 ($= 500$ and 1500 G), initial M_p ($= 0.7, 1, 1.5, 2 M_j$), and initial e ($e_i = 0, e_c - 0.01$, and e_c) in our simulations to investigate the fate of the planet migration under the influence of the cavity size, planet mass, and orbital eccentricity.

Two sizes of magnetospheric cavities are considered to approximately match the bimodal distribution of spin periods of young stars in the Orion Nebula Cluster. The initial $a_{2:1}$ corresponding to the large (small) cavity opened up by the stronger (weaker) stellar fields is ~ 0.045 AU (~ 0.032 AU). In the case of the large cavity ($B_0 = 1500$ G), the planets require nonzero e_i to enhance their tidal and magnetic interactions with their central stars and make significant inward migration. The migration rate increases with e_i for a given planet mass. When e_i is as large as the critical value e_c , R_p exceeds R_l and the Roche overflow occurs. For planets with different masses, massive planets

($M_p > 1M_j$) have higher e_c (i.e. more intense tidal heating) than less massive ones ($M_p \leq M_j$) because massive planets are more difficult to thermally inflate due to their greater gravitational binding energies and cooling rates. As a result, stronger stellar tides raised by the planet with higher M_p and e_i allow for faster migration. Overall, massive planets can therefore migrate further in than less massive ones, as shown in the simulations for $e_i = e_c - 0.01$. When $e_i = e_c$, low-mass planets ($M_p = 0.7$ and $1 M_j$) inflate by tidal heating faster than inward migration. Hence they overflow their large Roche lobes at large a , resulting in the low density and therefore the runaway mass loss. On the other hand, the high-mass planets ($M_p = 1.5$ and $2 M_j$) migrate inwards fast without significant tidal inflation. In contrast to the low-mass planets, once these planets fill their small Roche lobe at small a , their density is high enough that they can undergo stable L1 overflow. During this phase, tidal and magnetic interactions instead of tidal inflation drive them to lose mass, expand, and migrate outward. This stable mass-loss phase proceeds until these outward migrating planets are large enough to become unstable against mass loss. Finally, they lose all gas to their central stars.

In the case of the small cavity ($B_0 = 500$ G), the simulated planets in circular orbits all quickly migrate in due to the fierce tidal and magnetic interactions until they stably overflow their Roche radii. After that, they can move outwards due to the mass loss and move inwards again by the tidal and magnetic torques. As their mass goes down and their degeneracy is lifted, all of these planets are finally destroyed, suffering from the runaway mass loss as in the large-cavity case.

To study the significance of the magnetic interactions between the star and the planet in our model, we also simulate the cases by shutting down the interaction (i.e. $\epsilon = 0$). We found that the migration of less massive planets is more sensitive to the magnetic interaction, which is enhanced by their easily inflated radii. Setting $\epsilon = 0$ makes the migration rate of low-mass planets slower, as shown in the case for $M_p = 0.7M_j$ with $e_i = 0.21$ in the large-cavity case. By contrast, the inward migration of massive planets is less sensitive to the magnetic interaction but more to the tidal interaction. As has been summarized in the preceding paragraph, all planets in the small cavity destruct under both the tidal and magnetic torques at such close-in initial positions from the stars even if $e_i = 0$. When $\epsilon = 0$, only the planet of $0.7M_j$ can survive unless the low-mass planet starts with an eccentric orbit with $e_c = 0.18$.

The model presented here for the orbital evolution of young hot Jupiters is different from the works by Gu et al. (2003) and Trilling et al. (1998). In this work, we employ simple models including the star-planet interactions and disk locking, which are not considered by Gu et al. (2003). Furthermore, we take into account the planet expansion due to the adiabatic mass loss and model the mass loss rate using the approach in Kolb & Ritter (1990), whereas Gu et al. (2003) ignore the radius adjustment to the mass loss and use a free parameter to control the mass loss rate. Ignoring the mass-radius relation during the Roche-lobe overflow phase as done in Gu et al. (2003), a Roche-lobe filled giant planet with $e_i = e_c$ continuously loses its mass via tidal inflation and migrates outwards until the tidal heating rate is weaker than the cooling rate, leading to a survived planet of lower mass. On the other hand, Trilling et al. (1998) consider young hot Jupiters moving

inwards via the Type II migration without a magnetospheric cavity and tidal inflation. In their work including the mass-radius relation, once the planets of mass $< 3.36M_j$ get close enough to their central stars and therefore overflow their Roche lobes, they migrate outwards and finally lose all their mass onto the star. In this regard, our results are compatible with theirs. One of the major differences is that the mass loss is driven by the Type II migration in the model by Trilling et al. (1998), while in our work the mass loss is driven by the loss of orbital angular momentum via the tidal and magnetic interactions with the parent star whose spin is almost locked by the disk. Moreover, the planets of mass $\leq 2M_j$ with $e_i < e_c$ survive in the cavity during the CTTS phase in our model.

For the last few years, transit surveys have revealed the peculiar $M_p - a$ correlation for hot Jupiters: less massive hot Jupiters (< 1 Jupiter mass) are almost absent within ~ 0.03 AU from their parent dwarf stars of the ages \sim Gyrs. Our results show that during the CTTS phase, planets of $M_p \geq 1M_j$ with modest initial eccentricities ($e_i \gtrsim 0.3$) and sufficient magnetic interactions in a large cavity can migrate to $a < 0.03$ AU, while planets of $M_p < 1M_j$ cannot. More specifically, given $e_i < e_c$, the planet of $2M_j$ can safely arrive at $a \lesssim 0.024$ AU and the planet of $1.5M_j$ can get to $a \lesssim 0.025$ AU in the end of our simulations. Whether or not these planets can further migrate toward their spun-down parent stars during the main-sequence phase depends on Q'_* , which is not yet well understood.

Ogilvie & Lin (2007) suggested that Q'_* induced by hot Jupiters may become large (i.e. $\gg 10^6$) as CTTSs evolve to main-sequence stars based on their dynamical-tide model. As they and others (Pätzold & Rauer 2002; Jiang et al. 2003) pointed out, we would be extremely fortunate to observe these very close-in hot Jupiters if the current $Q'_* \sim 10^6$, implying that Q'_* of the solar-type main-sequence host stars may be quite large. However, it should be noted that these very close-in planets were all discovered by transit surveys (see Figure 1). Although transit surveys overall prefer to detect close-in planets (Gaudi et al. 2005), the detectability of a hot Jupiter as a function of the semi-major axis of interest here (i.e. $a \lesssim 0.05$ AU) is extremely ill-defined as the various transit surveys are subject to different observational limitations such as the transit depth, sampling rate, red noise, and detection threshold (Pont et al. 2006). If Q'_* indeed gradually becomes $\gg 10^6$ as CTTSs evolve to main-sequence stars, therefore allowing the planets to move a little bit inward during the short transition after $t = 10^7$ years while halting the further planet migration for most of the main-sequence phase, our model may have the potential to explain the absence of low-mass hot Jupiters within $a \lesssim 0.3$ AU.

On the other hand, a large body of studies have suggested that Q'_* associated with the tidal dissipation induced by the hot Jupiters in main-sequence dwarfs could be as small as $\sim 10^{5-6}$. As a result of the efficient tidal dissipation, the orbits of the hot Jupiters can decay so significantly that the planets may plunge into their host stars during the main-sequence phase (Jiang et al. 2003; Jackson et al. 2008). This “accretion” model may account for the paucity of the extremely close-in hot Jupiters concluded from radial-velocity surveys (Gaudi et al. 2005, also see Figure 1). In addition, the relatively young ages of the extremely close-in hot Jupiters revealed by transit surveys may

also lend support to the model (Jackson et al. 2009). Although the planet-metallicity correlation independent of the spectral type does not seem to favor the accretion model (Fischer & Valenti 2005), excessive heavy elements in the shallow convection zone of high-mass dwarfs may be able to sink down to the radiative zone via the double diffusive effect, thereby eliminating the metallicity enhancement and resolving the problem for the model (Vauclair 2004). Furthermore, Pont (2009) found an excess spin of the host stars of hot Jupiters, which may arise from tidal spin-up, although the uncertainty of the stellar ages and the limitation of a small number of samples demand more detections in the future to confirm the conclusion. The study by Jackson et al. (2009) for the accretion model is carried out based only on one-mass case (i.e. $1M_J$). If the accretion model is the main cause responsible for the observed $M_p - a$ relation, it would be expected that the extremely close-in giant planets of mass $< 1M_J$ of younger ages should also be detected by transit surveys. The orbital decay timescale during the main-sequence phase due only to the tidal dissipation is given by $t_{tide} \approx (J_0)/(2\dot{J}_*)$ (see equation(18)). In the case of a planet of $0.7M_J$, the planet can survive in $\sim 10^9$ yrs from the distance of $\sim 0.03\text{AU}$ at $t = 10$ Myrs. In contrast, the orbit of a planet of $2M_J$ will decay on the timescale of $\sim 10^7$ yrs from a distance of $\sim 0.025\text{AU}$ at $t = 10$ Myrs. In other words, during the main-sequence phase, less massive planets excite weaker tides on their parent stars and therefore still stay outside $a \sim 0.03$ AU, while the massive planets keep falling into the stars in the way as interpreted by Pätzold & Rauer (2002) and Jiang et al. (2003). The recently discovered hot Jupiter WASP-18b with an orbital period of 0.94 days and a mass of $10M_J$ may provide a constraint on Q'_* of a main-sequence star in the next few years (Hellier et al. 2009).

In this paper, we have attempted to bring several physical components to the context of the evolution of young hot Jupiters. Nonetheless, a large number of assumptions have been made to simplify the physical processes included in our model. The structure of the truncated disk is not modelled. How a planet migrates to $a_{2:1}$ and how the eccentricity evolves during its entry to the cavity (e.g. Rice et al. 2008) are not addressed. The disk accretion rate is assumed to be quasi-steady to determine the cavity sizes, while observations show otherwise (e.g. Baraffe et al. 2009). The dipole configuration of the stellar fields connecting to the disk ignores any types of winds even though the effect of disk locking is introduced in a simplified manner to imitate the sink of the total angular momentum in our model. The star-planet magnetic interactions are parameterized to scale with the Poynting flux at the magnetopause of the planet rather than appealing to any specific models, such as the dissipation due to the Alfvén waves and unipolar inductor (e.g. Zarka 2007) or induced by tilted stellar dipole fields (e.g. Laine et al. 2008; cf. Papaloizou 2007). The values of Q'_* and Q'_p chosen for the calculations are quite arbitrary; we have not explored a wide range of the values. The interior structure of an inflated planet and the mass-radius relation of a hot Jupiter are inferred from the 1-D numerical simulation (Bodenheimer et al. 2001; Gu et al. 2003) even for a Roche-lobe filled planet. Also, the code ignores thermal properties of the solid core of a giant planet, leaving a question as to what would happen to the core under the intense tidal heating. In a hot Jupiter-star system, the mass loss may occur via the Lagrangian 2 point as well (Gu et al. 2003), which is not considered in the present work. Besides, the mass loss from a planet in an

eccentric orbit may be intermittent and nonconservative, while the mass loss rate in our calculation is simply estimated from the L1 overflow at $r = a$. To use a more appropriate expression for the Roche radius and to consider the more realistic mass loss in asynchronous eccentric planetary systems, a more careful treatment (e.g. Sepinsky et al. 2007) is desired to refine the results. In light of these limitations and possible uncertainties, the simulations covering a wide range of the parameter space along with more realistic modelling on individual issues will be explored in a future work.

We are grateful to G. I. Ogilvie, F. Pont, and R. E. Taam for useful discussions. This work has been supported by the NSC grant in Taiwan through NSC 98-2112-M-001-011-MY2.

A. Appendix

The Roche radius R_l is defined as the distance between L1 and the planet’s center of mass. The conventional expression of R_l is derived from the circular restricted three-body problem (e.g. Murray & Dermott 1999). Gu et al. (2003) assumed that the Roche lobe overflow occurs around perihelion and made an approximation that $R_l = (M_p/3M_*)^{1/3}a(1 - e)$. Here we investigate the validity of the approximation by employing the expression for the L1 point in the elliptical restricted three-body problem (Todoran 1993). The exact values of the Roche radius in units of a are calculated using the equations in Todoran (1993) and are shown in Table 1 for various mass ratios and eccentricities relevant to our problem. The table shows that the Roche radius at perihelion is larger than that at aphelion in some of the cases. It is because the planet orbits faster (slower) than the “fictitious” circular motion performed at perihelion (aphelion). As a result, the centrifugal force due to the orbital motion is larger (smaller) at perihelion (aphelion) than the centrifugal force of the fictitious circular motion at the point, therefore enlarging (reducing) the Roche radius relative to the “Roche radius” associated with the circular motion.

Furthermore, the above analysis is based on the assumption that the spin of the planet is instantaneously synchronized with the orbit at any moment (Pratt & Strittmatter 1976). While it is true for a synchronized circular orbit, in an eccentric orbit the planet’s spin is normally “synchronized” with its orbital motion close to perihelion where the tidal forcing is expected to be near its maximum (Hut 1981; Ivanov & Papaloizou 2007; Langton & Laughlin 2008). Following the same line of the above argument, a “synchronized” planet spins faster than its orbit at aphelion, implying that the Roche radius is smaller than the value associated with the circular motion at the point.

It should be noted that equation (20) for the mass loss rate is also derived for a circular orbit. The equation should be modified as the L1 point changes its location along an eccentric orbit. Besides, when the planet’s photosphere is close to its time-varying Roche lobe in an eccentric orbit, the outer part of the planet should expand or contract with the Roche lobe on the local dynamical

timescale, which introduces additional complexity to estimate the mass loss rate.

It is for the above complex reasons that we simply use the expression $R_l = (M_p/3M_*)^{1/3}a$ to specify the Roche radius of a planet in an eccentric orbit in the present work.

REFERENCES

- Anderson et al. 2009, submitted to ApJ
- Armitage, P. J., & Clarke, C. J. 1996, MNRAS.280, 458
- Baraffe, I., Selsis, F., Chabrier, G., Barman, T. S., Allard, F., Hauschildt, P. H., & Lammer, H. 2004, A&A, 419, L13
- Baraffe, I., Chabrier, G., & Gallardo, J. 2009, ApJ, 702, 27
- Bodenheimer, P. Lin, D. N. C., & Mardling, R. A. 2001, ApJ, 548, 466
- Boss, A. 2004, ApJ, 610, 456
- Bouvier, J. 2007, IAUS, 243, 231
- Carr, J. S. 2007, IAUS, 243, 135
- Choi, P. I., & Herbst, W. 1996, AJ, 111, 283
- Davis, T. A., & Wheatley, P. J. 2009, MNRAS, accepted
- Fischer, D. A., & Valenti, J., ApJ, 622,1102
- Ford, E. B., & Rasio, F. A. 2008, ApJ, 686, 621
- Gammie, C. F., 2001, ApJ, 553, 174
- Gaudi, B. S., Seager, S., & Mallen-Ornelas, G., 2005, ApJ, 623, 472
- Gilliland R. L. 1986, ApJ, 300, 339

Table 1: Roche radius in units of a calculated for different mass ratios and eccentricities

M_p/M_*	e	Roche radius at perihelion (a)	Roche radius at aphelion (a)
2×10^{-3}	0.1	0.0851	0.0842
2×10^{-3}	0.3	0.0831	0.0833
1×10^{-4}	0.1	0.0411	0.0265
1×10^{-4}	0.3	0.061	0.0221

- Gu, P. G., Lin, D. N. C., & Bodenheimer, P. 2003, *ApJ*, 588,509
- Gu, P. G., Bodenheimer, P., & Lin, D. N. C. 2004, *ApJ*, 608,1076
- Hellier, C, Anderson, D. R., Cameron, A. C., Gillon, M., Hebb, L., Maxted, P. F. L., Queloz, D., Smalley, B., Triaud, A. H. M. J., West, R. G., Wilson, D. M., Bentley, S. J., Enoch, B., Horne, K., Irwin, J., Lister, T. A., Mayor, M., Parley, N., Pepe, F., Pollacco, D. L., Segransan, D., Udry, S., Wheatley, P. J. 2009, *Nature*, 460, 1098
- Herbst, W., & Mundt, R 2005,*ApJ*, 633.967
- Huélamo, N., Figueira, P., Bonfils, X., Santos, N. C., Pepe, F., Gillon, M., Azevedo, R., Barman, T., Fernández, M., di Folco, E., Guenther, E. W., Lovis, C., Melo, C. H. F., Queloz, D., & Udry, S. 2008, *A&A*, 489, 9
- Hut, P. 1981, *A&A*, 99, 126
- Ibgui, L., & Burrows, A. 2009, arXiv:0902.3998v1
- Ida, S. & Lin, D. N. C. 2004, *ApJ*, 604, 388
- Ivanov, P. B., & Papaloizou, J. C. B. 2007, *MNRAS*, 376, 682
- Jackson, B., Greenberg, R., & Barnes, R. 2008, *IAUS*, 249, 119
- Jackson, B., Barnes, R., & Greenberg, R. 2009, *ApJ*, 698,1357
- Jiang, I. G., Ip, W. H., & Yeh, L. C. 2003, *ApJ*, 582, 449
- Kokubo, E., & Ida, S. 2002, *ApJ*, 581, 666
- Kolb, U., & Ritter, H. 1990, *A&A*, 236, 385
- Laine, R. O., Lin, D. N. C., & Dong, S.-F. 2008, *ApJ*, 685, 521
- Langton, J., & Laughlin, G. 2008, *A&A*, 483, L25
- Lin, D. N. C., Bodenheimer, P., & Richardson, D. C. 1996, *Nature*, 380, 606
- Lin, D. N. C., & Papaloizou, J. C. B. 1985, in *Protostars and Planet II*, ed. D. C. Black & M. S. Matthews (Tuscon: Univ. Arizona Press), 981
- Livio, M., & Pringle, J. E. 1992, *MNRAS*, 259, 23
- Long M., Romanova M. M., & Lovelace R. V. E. 2005, *ApJ*, 634, 1214
- Lovelace, R. V. E., Romanova, M. M., & Barnard, A. W. 2008, *MNRAS*, 389, 1233
- Mardling, R. A. 2007, *MNRAS*, 382, 1768

- Mardling, R. A. & Lin, D. N. C. 2002, *ApJ*, 573, 829
- Marley, M. S., Fortney, J. J., Hubickyj, O., Bodenheimer, P., & Lissauer, J. J. 2007, *ApJ*, 655, 541
- Matt, S., & Pudritz, R. E. 2005 *ApJ*, 632, 135,
- Mayor, M., & Queloz, D. 1995, *Nature*, 378 355
- Miller, N., Fortney, J. J., Jackson, B. 2009, *ApJ*, 702, 1413
- Murray, C. D. & Dermott, S. F. 1999, *Solar System Dynamics*, Cambridge Univ. Press
- Murray-Clay, R., Chiang, E., & Murray, N. 2009, *ApJ*, accepted
- Nagasawa, M., Ida, S., & Bessho, T. 2008, *ApJ*, 678, 498
- Narita, N., Sato, B., Hirano, T. & Tamura, M. 2009 arXiv 0908.1673N
- Ogilvie, G. I., & Lin, D. N. C. 2007, *ApJ*, 661, 1180
- Papaloizou, J. C. B. 2007, *A&A*, 463, 775
- Pätzold, M. & Rauer, H. 2002, *ApJ*, 568, L117
- Pollack, J. B., Hubickyj, O., Bodenheimer, P., Lissauer, J. J., Podolak, M., & Greenzweig, Y. 1996, *Icarus*, 124, 62
- Pols, O. R., Tout, C. A., Eggleton, P. P., Han, Z. 1995, *MNRAS*, 274, 964
- Pont, F., Zucker, S., & Queloz, D. 2006, *MNRAS*, 373,231
- Pont, F. *MNRAS*, 396,1789
- Pratt, J. P., & Strittmatter, P. A., 1976, *ApJ*, 204, 29
- Rafikov, R. R. 2005, *ApJ*, 621, 69
- Rice, W. K. M., Armitage, P.J., & Hogg, D. F. 2008, *MNRAS*, 384, 1242
- Romanova, M. M. & Lovelace, R. V. E. 2006, *ApJ*, 645, 73
- Sepinsky, J. F., Willems, B., & Kalogera, V. 2007, *ApJ*, 660, 1624
- Setiawan, J., Henning, Th., Launhardt, R., Muller, A., Weise, P., & Kurster, M. 2008, *Nature*, 451, 38
- Shu, F., Najita, J., Ostriker, E., Wilkin, F., Ruden, S., & Lizano, S, 1994, *ApJ*, 429, 781
- Starczewski, S., Gawryszczak, A. J., Wunsch, R., & Rozyczka, M. 2007, *AcA*, 57,123

Symington, N.H. Harries, T.J., Kurosawa, R., & Naylor, T. 2005, *MNRAS*, 358, 977

Todoran, I. 1993, *Ap&SS*, 199,257

Trilling, D. E., Benz, W., Guillot, T., Lunine, J. I., Hubbard, W. B., & Burrows, A. 1998, *ApJ*, 500, 428

Udry, S., & Santos, N. C. 2007, *Annu. Rev. Astron. Astrophys.*, 45, 397

Vauclair, S. 2004, *ApJ*, 605, 874

Zarka, P. 2007, *Planetary and Space Science*, 55(5), 598

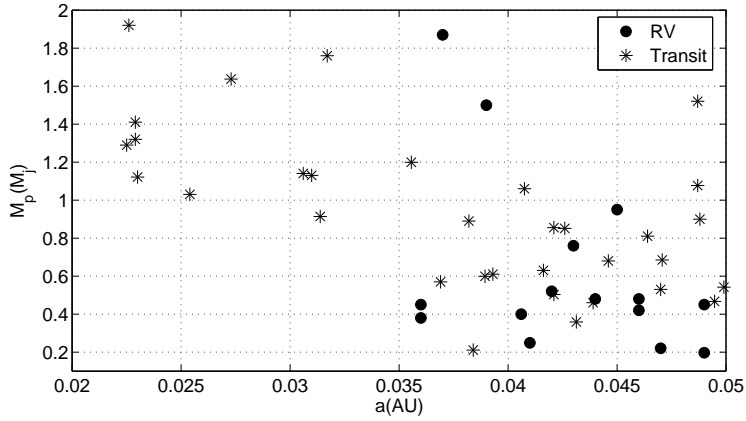


Fig. 1.— The semi-major axis vs. mass relation for the hot Jupiters of mass between 30 Earth masses and 2 Jupiter masses. The data are adopted from the website <http://exoplanet.eu/>. The transiting exoplanets are shown by the asterisks and the exoplanets discovered in radial velocity surveys are denoted by the black circles. The exoplanets that are known to be in retrograde orbits are excluded in the plot because their orbital orientations are unlikely to be explained by the planet migration model as presented in this paper (Nagasawa et al. 2008; Anderson et al. 2009; Narita et al. 2009).

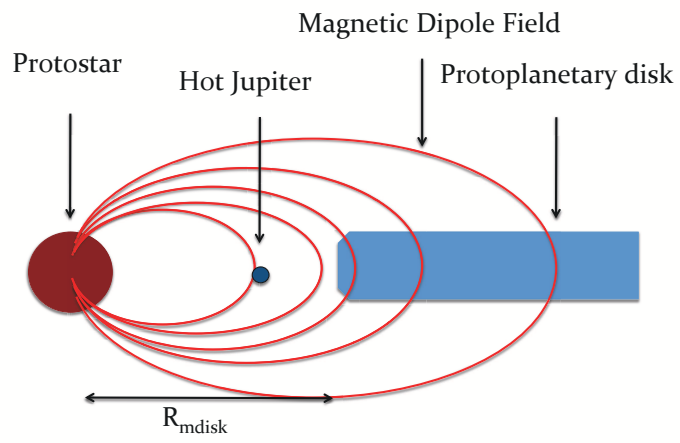


Fig. 2.— A schematic illustration of our simple model.

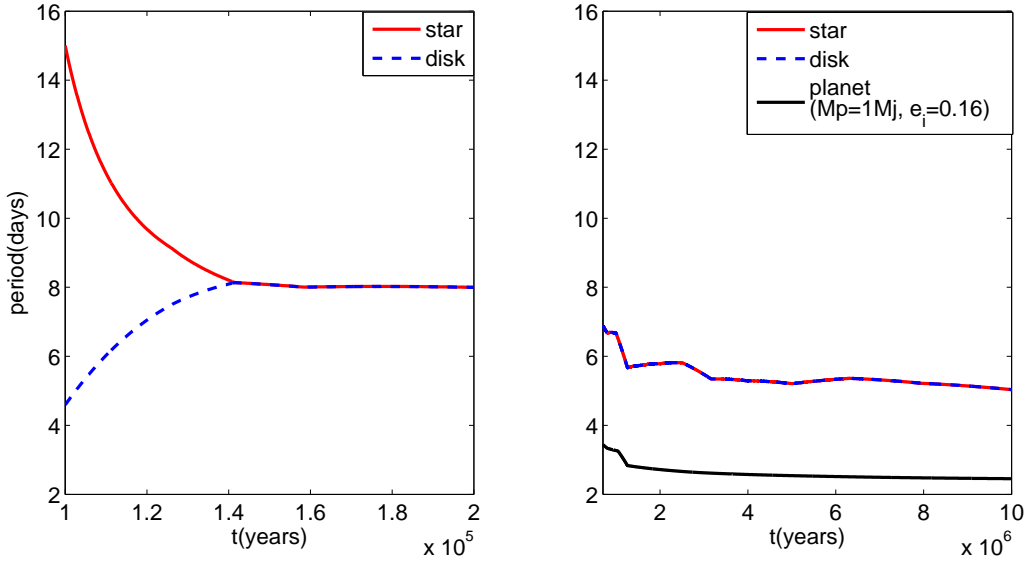


Fig. 3.— The evolution of the stellar spin (red line), the rotational period of the inner edge of the disk (blue dashed line), and the orbital period of the planet (black line). The left panel displays that the star’s initial spin period (i.e., 15 days) at $t = 10^5$ years is locked to 8 days by the disk in $\sim 4 \times 10^4$ years. Afterwards, the star corotates with the disk inner edge, and its spin rate is determined by the disk accretion and the disk locking. The planet’s orbital period is added in the right panel to compare to the stellar spin period and the rotational period of the inner edge after the planet is introduced at $t = 7 \times 10^5$ years. The difference between the planet’s orbital and stellar spin rates leads to the planet’s inward migration as shown by the black curve, while the star does not spin up via the tidal effect and star-planet magnetic linkage due to the strong disk locking.

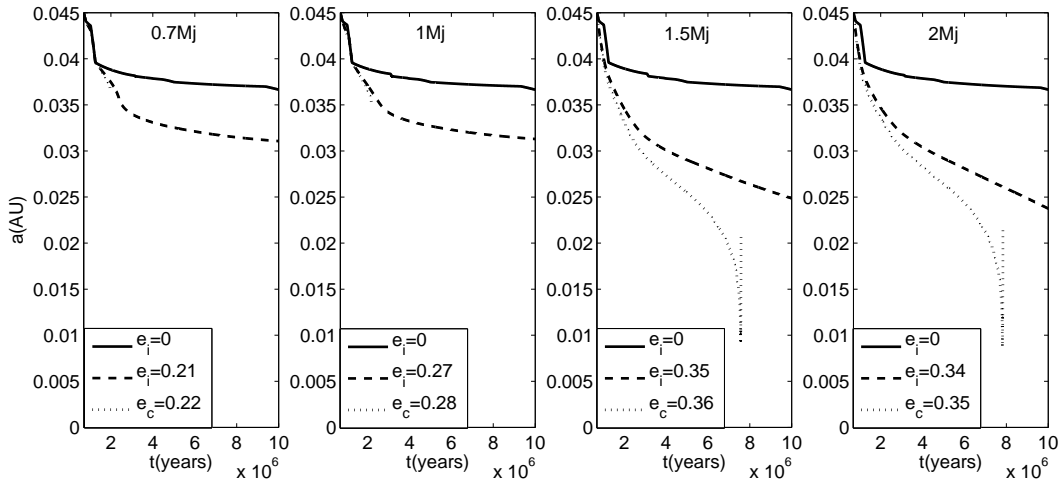


Fig. 4.— Orbital evolutions of the planets in the large cavities. By modulating the initial eccentricity, the orbital evolution will change. Each panel displays the results for a different initial M_p . The solid line demonstrates the orbital evolution of the planet with $e_i = 0$; the dashed line illustrates the case in which the planet of a given initial mass can migrate the longest distance; the dotted line shows that the planet with $e_i = e_c$ destructs at the breaking point.

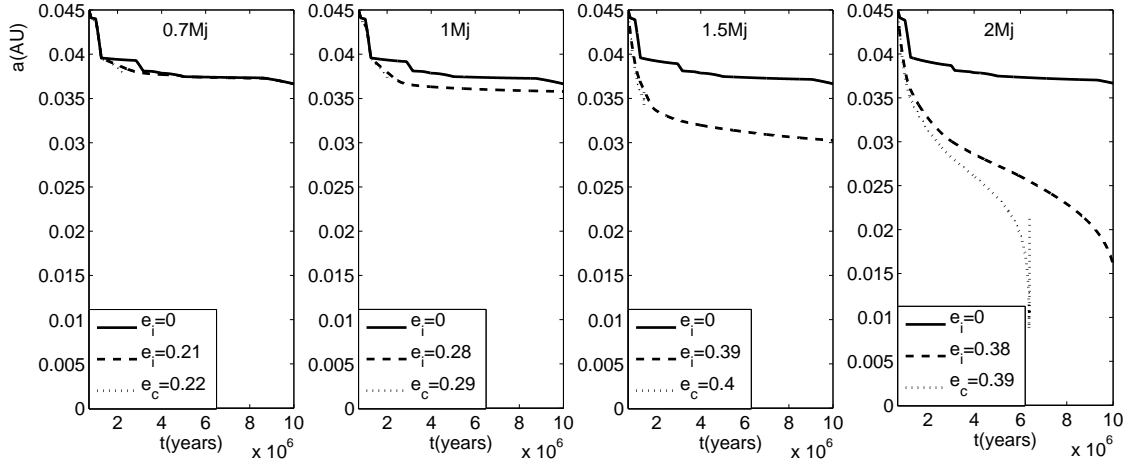


Fig. 5.— The same as Figure 4 except that the coefficient ϵ is reduced to 0, meaning that the magnetic fields do not exert any torque on the planet. The critical eccentricities e_c are relatively high compared to the previous cases for $\epsilon = 1$.

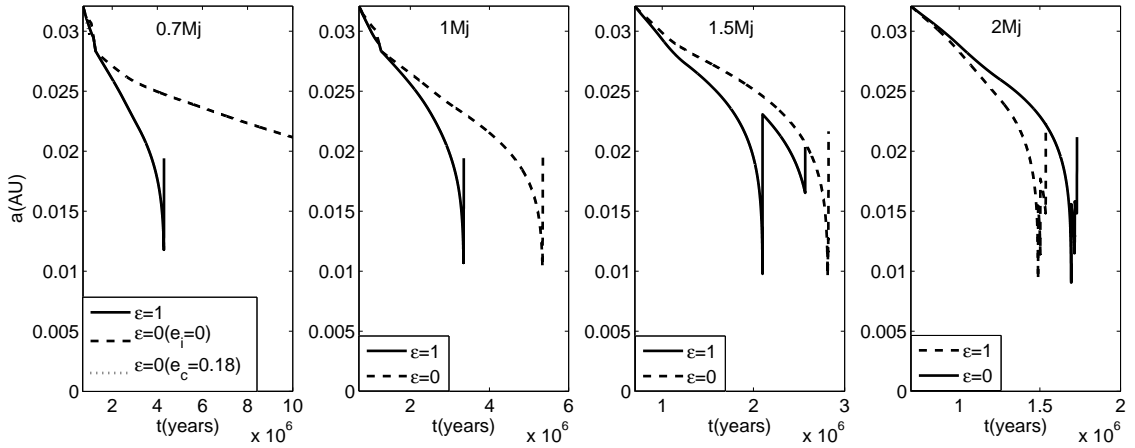


Fig. 6.— Comparison between the cases with the magnetic torque in full strength ($\epsilon = 1$ plotted in solid line) and without the magnetic torque ($\epsilon = 0$ plotted in dashed line) for the orbital evolutions of the planets of different masses with $e_i = 0$ in the small cavities. Note that since the planet of $0.7M_j$ with $e_i = 0$ survives up to the end of the simulation at $t = 10^7$ yr, its e_c is estimated and the corresponding evolution is also shown (dotted line) in the leftmost panel.